Published in final edited form as:
Nat Chem Biol. 2020 April 01; 16(4): 469–478. doi:10.1038/s41589-020-0483-3.

A widespread role for SLC transmembrane transporters in resistance to cytotoxic drugs

Enrico Girardi[1], **Adrián César-Razquin**[1], **Sabrina Lindinger**[1], **Konstantinos Papakostas**[1,#], **Justyna Konecka**[1], **Jennifer Hemmerich**[2], **Stefanie Kickinger**[2], **Felix Kartnig**[1], **Bettina Gürtl**[1], **Kristaps Klavins**[1], **Vitaly Sedlyarov**[1], **Alvaro Ingles-Prieto**[1], **Giuseppe Fiume**[1], **Anna Koren**[1,3], **Charles-Hugues Lardeau**[1,3], **Richard Kumaran Kandasamy**[1,4], **Stefan Kubicek**[1,3], **Gerhard F. Ecker**[2], **Giulio Superti-Furga**[1,5,*]

[1]CeMM Research Center for Molecular Medicine of the Austrian Academy of Sciences, Vienna, Austria

[2]Department of Pharmaceutical Chemistry, University of Vienna, Vienna, Austria

[3]Christian Doppler Laboratory for Chemical Epigenetics and Antiinfectives, CeMM Research Center for Molecular Medicine of the Austrian Academy of Sciences, Vienna, Austria

[4]Department of Clinical and Molecular Medicine, Norwegian University of Science and Technology, Trondheim, Norway

[5]Center for Physiology and Pharmacology, Medical University of Vienna, Vienna, Austria

Abstract

Solute Carriers (SLCs) represent the largest family of transmembrane transporters in humans and constitute major determinants of cellular metabolism. Several SLCs have been shown to be required for the uptake of chemical compounds into cellular systems, but systematic surveys of transporter-drug relationships in human cells are currently lacking. We performed a series of genetic screens in a haploid human cell line against 60 cytotoxic compounds representative of the chemical space populated by approved drugs. By using an SLC-focused CRISPR/Cas9 library, we identified transporters whose absence induced resistance to the drugs tested. This included dependencies involving the transporters SLC11A2/SLC16A1 for artemisinin derivatives and SLC35A2/SLC38A5 for cisplatin. The functional dependence on SLCs observed for a significant proportion of the compounds screened suggests a widespread role for SLCs in the uptake and cellular activity of cytotoxic drugs and provides an experimentally validated set of SLC-drug associations for a number of clinically relevant compounds.

[*]Corresponding author: Giulio Superti-Furga, CeMM Research Center for Molecular Medicine of the Austrian Academy of Sciences Lazarettgasse 14, AKH BT25.3, 1090 Vienna, Austria, gsuperti@cemm.oeaw.ac.at, Telephone: +43 1 40160 70 001.
[#]Current Address: ViruSure GmbH, Tech Gate Vienna, Donau-City-Strasse 1A - 1220 Vienna

Author contributions

E.G., G.S-F. conceived and designed the study. E.G., K.P., S.L., J.K., B.G., K.K., G.F., A.I. P., F.K., A.K. and C-H.L. performed experiments and analyzed data. A.C-R analyzed screening and validation data. V.S. analyzed the transcriptomics data. J.H, S.Ki. and G.F.E. performed the chemoinformatic analysis. R.K.K. contributed to library design. S.Ku., G.F.E. and G.S-F. provided supervision.

Competing Financial Interests Statement

The authors declare no competing financial interests. C-H. L. is an employee of AstraZeneca Limited (UK).

Europe PMC Funders Author Manuscripts

Introduction

Cellular metabolism influences the rates of drug uptake and extrusion/excretion through the action of transmembrane transporters, the availability of cofactors and target(s), and the processing of prodrugs into active forms[1]. Moreover, drug modifying enzymes (DMEs), such as members of the cytochrome p450 family and glucosyltransferases, add functional groups to xenobiotic compounds, facilitating their removal from the cell and eventually the organism[1]. Most of what is known about the uptake of drugs by membrane-bound transporters stems from the analysis of drug disposition in the kidney, liver, intestine and blood-brain-barrier, with a focus on the entry and exit of pharmacological agents from the blood circulation[2,3]. In particular, two main families of transporters have been previously shown to directly interact with drugs: ATP-binding cassette transporters (ABCs)[4] and Solute Carrier proteins (SLCs)[3,5]. ABC transporters are generally involved with the export of drugs, while SLCs have been mostly described to be involved in compound uptake even though exceptions to this rule exist, such as in the case of the MATE (multidrug and toxic compound extrusion) transporters[6]. Notably, SLCs represent a largely understudied family, counting more than 400 members of which at least 30% are still considered entirely orphan[3]. SLCs are divided into subfamilies based on sequence similarity and have been shown to transport a variety of molecules, ranging from nucleotides, sugars and lipids to amino acids and peptides[3,5], often with overlapping specificities. Consistent with their critical role in drug absorption and excretion, considerable knowledge has accumulated on a few large subfamilies of SLCs prevalently expressed in kidney, liver and intestine, such as the SLC22 and SLCO families[7,8]. There is ample consensus in ascribing an important role for these transporters in affecting pharmacokinetics of several drugs, which has been corroborated by a number of pharmacogenomic polymorphisms[9]. Accordingly, the US Food and Drug Administration and the European Medicines Agency currently recommend the testing of several ABC and SLC22/SLCO members for clinical drug interaction studies[10]. However, it remains a matter of debate to which extent membrane-bound transporters are involved in the uptake and metabolism of drugs at the target cell level, such as in muscle, brain or tumor cells[11–13]. Some drugs have been reported to depend on protein carriers to enter cells, with prominent cases such as the nucleoside transporter SLC29A1/ENT1 (equilibrative nucleoside transporter 1) interacting with several nucleoside analogs such as clofarabine, gemcitabine and fluorouracil[14]. In parallel, modulation of transporter activity or expression levels has been shown to affect the efficacy of drugs, independently from direct uptake events, through their effects on cellular metabolic processes such as glycolysis and oxidative phosphorylation[15,16].

Genetic screening offers a powerful tool to identify both direct and indirect interactions between a gene and a specific phenotype. Using insertional mutagenesis, we recently demonstrated that the presence of the intact *SLC35F2* gene was the major determinant of the uptake of sepantronium bromide (YM155), a small molecule displaying anti-tumor activity *in vitro* and *in vivo*, in a variety of cell lines[17]. Similar forward genetics approaches have previously led to the identification of transporters involved in the uptake of cytotoxic compounds such as tunicamycin and 3-bromopyruvate[18,19]. Given the lack of molecular reagents available for the solute carrier family[3], only recently have modern human cell

genetic approaches allowed us to test the hypothesis that SLC-mediated drug action, generally through uptake, is rather the rule than the exception. To tackle this important question in a focused way, we used an SLC-specific CRISPR/Cas9 KO library to perform a systematic genetic survey of transporters involved with a chemically diverse set of 60 cytotoxic drugs. We identified and validated a large number of SLC-compound associations, providing insights into both direct uptake events and indirect associations affecting the metabolism and mechanism of action of the drugs tested. Importantly, a large proportion of the compounds screened showed an association with at least one SLC, suggesting that this class of proteins plays a large and only partially understood role in determining uptake and activity of clinically relevant compounds.

Results

Generation of an SLC-specific CRISPR/Cas9 library

In order to investigate SLCs in an unbiased manner, we constructed a CRISPR/Cas9 library targeting 394 human SLC genes and pseudogenes with six single guide RNAs (sgRNAs) per gene. Particular care was taken to avoid sgRNAs with sequences sharing similarity with other SLC or ABC transporters. A set of negative control sgRNAs (predicted not to target any sequence in the genome) as well as a set of sgRNAs targeting genes scoring as essential in HAP1 and KBM7 cell lines based on previous insertional mutagenesis data[20] were also included in the pool (Fig. 1a, Supplementary Table 1). The resulting library consisted of 2,609 unique sgRNAs, allowing for highly scalable and multiplexable screening and sequencing protocols. Presence of all sgRNAs was confirmed by Next Generation Sequencing (NGS, Supplementary Fig. 1a). Comparison of plasmid samples with HAP1 cell genomic DNA samples taken nine days post-infection showed significant depletion of sgRNAs targeting the set of essential genes (54/120, p-value = 8.2×10^{-26}, Fisher's exact test, Supplementary Fig. 1b). No significant depletion or enrichment was observed for the set of negative control sgRNAs (21/120, enrichment p-value = 0.29, depletion p-value = 1, Fisher's exact test, Supplementary Fig. 1c). At the gene level, we identified several SLCs important for optimal fitness of HAP1 cells, including SLC35B1, the recently deorphanized ATP/ADP exchanger in the endoplasmic reticulum[21], and MTCH2, a mitochondrial carrier involved in the regulation of apoptosis and a repressor of mitochondrial metabolism[22] (Supplementary Fig. 1d). To validate the efficiency and specificity of our library in detecting SLCs associated with drug action, we screened for SLC genes responsible for resistance to YM155. Screening in HAP1 cells with 200nM YM155 for 72h resulted in a clear enrichment of sgRNAs targeting the SLC35F2 gene (Supplementary Fig. 1e). While potential off-target effects of the sgRNAs used cannot be completely excluded, these results point to a high degree of specificity in our library and confirm that SLC35F2 is the sole SLC responsible for YM155 resistance, consistent with our previous findings derived from insertional mutagenesis experiments[17].

The SLC repertoire of HAP1 cells

Immortalized human cell lines typically express 150-250 SLC genes, with abundancy patterns resembling those of tissues[23,24]. For our screen, we chose HAP1 cells, a human cell line bearing considerable technical advantages. HAP1 cells express 207 human SLC genes,

as assessed by transcriptional profiling using RNA-Seq (Supplementary Fig. 1f). Importantly, these cells do not express most members of the organic ion transporter SLC22 family that have been implicated in the uptake of drugs in kidney, gut and liver[7], making it ideally suited to test the potential role of other SLC families. Moreover, by being haploid, loss-of-function phenotypes induced by CRISPR/Cas9 technology should be more easily interpretable, as they do not represent composite mutants of different alleles.

Identification of a set of cytotoxic drugs

For our genetic screens, we aimed at selecting a set of compounds representative of the chemical and functional space populated by drugs. We therefore tested cytotoxicity of an initial set of 1812 compounds (2k library) including the CLOUD library[25] and the NIH Clinical Collection as well as sets of epigenetic modifiers and toxic compounds. A subset of 270 (14.9%) compounds was found to be cytotoxic in HAP1 cells at the tested concentration (toxic set) (Fig. 1b). This set was complemented by an additional group of drugs with underrepresented indications e.g. compounds involved in DNA-damage-based-sensitivity, and eight-point dose-response curves were subsequently measured for each compound in order to determine IC_{50} values. Finally, a group of 60 compounds chosen to cover different target classes and focusing on drugs with clinical relevance and diverse indications was selected for screening with the CRISPR/Cas9 library (screen set, Fig. 1b-c, Supplementary Table 2).

Identification of known and novel SLC-drug associations

We infected haploid HAP1 cells with the SLC CRISPR/Cas9 library to generate a pool of cells each lacking one specific SLC. The population was treated for 72h with multiple concentrations of the cytotoxic compounds, generally one, three and ten times the measured IC_{50}. As expected by dosing cytotoxic drugs, we retrieved all the samples treated with the IC_{50} concentrations as well as 78% (35/45) of the treatments at 2-3X the IC_{50} and 37% (22/60) of the 10X IC_{50} treatments. Enrichment was first calculated at the sgRNA level using DESeq2 (Fig. 2a) and then aggregated at the gene level using the GSEA algorithm (Fig. 2b). When positive enrichment for SLC genes was calculated, we identified 201 SLC/drug associations involving 47 drugs (76 different treatment modalities) and 101 SLCs (Fig. 2c, Supplementary Fig. 2a-b, Supplementary Table 6) at a False Discovery Rate (FDR) ≤ 1%. We observed enrichments up to ~8 log2 (fold change) with most interactions showing mild enrichments (Fig. 2c, Supplementary Fig. 2c). While we observed cases of drugs interacting with more than 10 SLCs, most compounds showed enrichments for only one or two genes (Supplementary Fig. 2d). Most of the SLCs identified are expressed in HAP1 cells (93/101, 92%, Supplementary Fig. 2e), with the remaining eight transporters likely showing expression only after lentiviral infection. A large proportion of the 101 SLCs identified in our screen are reported to localize at the plasma membrane (Supplementary Fig. 2f).

Rewardingly, drugs belonging to the same classes generated prominent clusters. One example is represented by the cluster of the antifolate drugs methotrexate, raltitrexed and pralatrexate, which all induced a strong enrichment in KOs of the reduced folate carrier SLC19A1/RFC. This transporter has been previously recognized as the main uptake route of

these antimetabolites into cells[26]. In particular, pralatrexate was developed to exploit this entry route[27] and it showed exclusive enrichment for SLC19A1 in our screen (Fig. 2c). Interestingly, within this cluster we found the structurally unrelated drug pentamidine, which is used for the treatment of African trypanosomiasis and leishmaniasis, as well as for the prevention and treatment of pneumocystis pneumonia (PCP) in immunocompromised patients. The mechanism of action (MoA) of this drug is poorly understood but earlier reports suggested it might be involved with inhibition of the parasite dihydrofolate reductase[28]. Another cluster included the nucleoside-like drugs decitabine, cytarabine, 5-azacytidine and gemcitabine, which all showed enrichment for the nucleoside transporter SLC29A1/ENT1 (Fig. 2c). SLC29A1 was previously reported to act as an importer of these compounds[14]. As HAP1 cells express very low levels or do not express the additional nucleoside transporters SLC29A2, SLC28A1 and SLC28A3 (Supplementary Fig. 1f), loss of SLC29A1 is expected to result in an impaired uptake of these compounds within the cell. For some (i.e. cytarabine and decitabine), but not all of these compounds, we detected enrichment of the mitochondrial phosphate/copper transporter SLC25A3 (Fig. 2c).

We also observed more exclusive interactions, such as the one between the antineoplastic drug mitoxantrone and the two transporters SLC47A1/ MATE1 and SLC47A2/ MATE2 (Fig. 2c). While mitoxantrone, a type II topoisomerase inhibitor and DNA intercalating agent, was previously reported to also inhibit the uptake/efflux of SLC47A1/ MATE1 substrates[29], our findings suggest that the interaction of this compound with these transporters may be associated with their uptake.

Moreover, we observed several cases of interactions offering plausible insights in the MoA or metabolic impact of a drug treatment. The artemisinin-derivatives artesunate and dihydroartemisinin showed an enrichment for the SLC11A2 and SLC16A1 genes (Fig. 2c). These compounds, generally used for the treatment of malarial infections, have recently found additional use as antineoplastic agents[30]. Although the MoA is not fully understood, their cytotoxicity appears to rely on an iron/heme-dependent activation step and subsequent generation of Reactive Oxygen species (ROS)[31]. SLC11A2, also known as DMT1 (divalent metal transporter 1), is a metal transporter which has been shown to control the pool of cytoplasmic iron[32], therefore affecting the drug activation step or the level of hydroxyl radicals in the cell[33]. SLC16A1, also known as MCT1 (monocarboxylate transporter 1) is a major lactate exporter that plays an important role in glycolytic metabolism[34] and could be directly involved in drug uptake or affect the ROS response to these compounds. Finally, we also observed a strong enrichment of the transporters SLC35A2, a nucleoside-sugar Golgi transporter[35], and SLC38A5, an amino acid transporter[36], upon treatment with the DNA-damaging agent cisplatin (Fig. 2c). Overall, the experimental drug-SLC gene interaction map showed a remarkably large landscape of known and novel associations covering 35 different SLC subfamilies, representing almost two thirds of the total of subfamilies tested.

Validation of selected SLC-drug associations

While the screen was effective in determining a genetically defined functional relationship, it did not reveal the degree and the kinetics by which loss of function of an individual SLC affected loss of cell growth compared to an isogenic cell. We selected a set of 33 SLC-drug

interactions (Supplementary Table 3), involving 21 drugs and 13 SLCs, to assess growth differences in pairwise comparisons. We applied a FACS-based Multicolor Competition Assay (MCA), where HAP1 cells carrying an sgRNA targeting a given SLC (Supplementary Table 4) and an enhanced GFP (eGFP) expression construct were mixed at 1:1 ratio with cells carrying a control sgRNA (targeting the *Renilla spp luciferase* gene, not present in the cells) and an mCherry construct (Supplementary Fig. 3a). The mixed population was then treated with either vehicle or the cytotoxic compound at 1-3 times the IC_{50} and the ratio of GFP+/mCherry+ determined by FACS three and ten days later (Fig. 3a). Two sgRNAs were used for each gene targeted in order to control for sgRNA-specific effects. Overall, this approach enabled the validation of several of the strongest interactions derived from the genetic screen (Fig. 3b, Supplementary Fig. 3b, Supplementary Table 7). In particular, we confirmed the strong effects of SLC19A1 and SLC29A1 loss on the resistance to antifolate and nucleoside analogs at both early (3 days) and late (10 days) timepoints. In addition, we validated the effect of the loss of SLC20A1, a phosphate transporter, upon pentamidine treatment. We also observed strong and time-dependent enrichments of cells lacking SLC11A2 or SLC16A1 upon treatment with artesunate and dihydroartemisinin, as well as in the case of panobinostat and the amino acid transporter SLC1A5. Finally, we observed strong enrichments of SLC35A2- and SLC38A5-lacking cells upon cisplatin treatment. This effect was already discernible for SLC38A5 after three days of drug exposure and became clear for both genes after ten days. Overall, we were able to confirm the majority (21/33) of the associations tested at one or more timepoints, therefore validating the approach and results of the genetic screen.

Direct and indirect effects of SLCs on drug sensitivity

To investigate the mechanisms by which SLCs can affect cell sensitivity to cytotoxic compounds, we further validated the interactions between the antifolate methotrexate and SLC19A1 as well as the interaction between artesunate and SLC16A1 (Fig. 4). To confirm the methotrexate-SLC19A1 interaction, we made use of two single cell-derived HAP1 cell lines carrying frameshift mutations in this gene (ΔSLC19A1_1, ΔSLC19A1_2). In a luminescence-based viability assay, we observed increased resistance of these cell lines to methotrexate-induced cell death (Fig. 4a). We also measured the intracellular concentration of the drug in WT and SLC19A1-deficient cells by LC-MS/MS, observing greatly reduced concentrations for the latter (Fig. 4b). This result is consistent with the reported role of SLC19A1 as methotrexate transporter[26], providing evidence of a direct effect of the SLC on this compound. We then investigated the interaction between artesunate and SLC16A1 (Fig. 4c-f). SLC16A1-deficient cell lines showed increased resistance to artesunate treatment compared to WT cells (Fig.4c). Importantly, ectopic expression of an SLC16A1 cDNA resulted in reduced resistance to artesunate compared to control cell lines ectopically expressing eGFP (Fig. 4d-e), demonstrating that SLC16A1 protein levels affect cell resistance to artesunate. However, intracellular concentrations of artesunate were not affected by loss of SLC16A1 and, while a reduced drug concentration was observed upon expression of the ectopic constructs, this did not vary between transporter-expressing and GFP-expressing cells (Fig. 4f). In an attempt to gain further insights into the metabolic rearrangements induced by cytotoxic compound treatment, we measured transcriptomic changes upon treatment with artesunate or cisplatin for 24h at IC_{50} in both WT and SLC-

deficient cells (SLC11A2- and SLC16A1-deficient cells for artesunate, SLC35A2- and SLC38A5-deficient cells for cisplatin, Supplementary Fig. 4a-b). Upon inspection of the transporter differential expression levels, we observed that artesunate treatment induced the upregulation of several amino acid transporters including SLC7A11/SLC3A2, SLC1A4 and SLC6A9 (Supplementary Fig. 4a). Further analysis for enrichment of transcription factor target genes identified the gene set regulated by ATF3 and ATF4 as significantly enriched upon drug treatment (Supplementary Fig. 4c-h), consistent with the upregulation of stress response-related proteins previously described upon treatment with this compound[37,38]. Interestingly, a similar pattern was detected for cisplatin-treated cells (Supplementary Fig. 4a, 4d), in line with the previously reported role of ATF3/4 as mediators of cisplatin-mediated toxicity[39]. No clear differential response was however detected between WT and SLC16A1-deficient cells upon artesunate treatment (Supplementary Fig. 4b, 4f), suggesting the increased resistance observed in the SLC-deficient cells is not due to a transcriptional response but might rather be due to post-translational effects or changes in the metabolic state of the cell.

Comparison of compound sets to the drug chemical space

The remarkable finding that so many drugs showed a functional dependence on an SLC transporter raised the question whether the functional landscape tested is biased for particularly properties (e.g large and hydrophilic compounds) and not representative of the general drug-like chemical space. We therefore decided to perform a detailed cheminformatics analysis in order to assess the representativeness of the compounds sets used in our screen. DrugBank 5.1.1[40] was taken as a reference of the known drug chemical space and compared to all three aforementioned compound sets (2k library, toxic and screen, Fig. 1b, Fig. 5a). All sets were curated according to the same protocol (see methods) and 22 physicochemical 2D descriptors (Supplementary Table 5) were calculated for every compound. Principal components (PC) analysis based on these descriptors showed a substantial overlap of the drug-like space represented by DrugBank and the initial 2k library, with the other two smaller subsets (toxic and screen set) spreading within the area of highest density (Fig. 5b-c, Supplementary Fig. 5a). In particular, the first and the second PCs were able to explain 62.1% of the variance of the data, with descriptors contributing the most including number of heavy atoms, molecular weight, Labute's surface area, number of heteroatoms, number of saturated rings, number of H-bond donors and polar surface area (TPSA, Fig. 5b-c). Additionally, comparison of the distributions of individual descriptors across compound subsets, and in particular those contributing the most to the variance of PC 1 and 2 (Fig. 5b), did not show important differences (Supplementary Fig. 6). Although a slight trend towards bigger molecules in the screen subset versus DrugBank was observed, this is likely due to the pronounced skewness of DrugBank in combination with the comparably small sample size of the subsets, and it did not result in any particular different distribution in the PCA. Overall, this analysis showed that there is no striking difference in the distribution of physicochemical properties of the compound sets used in this study, and hence the final screen set can be considered representative of the general drug chemical space.

Moreover, we additionally compared the chemical properties of the set of 47 compounds associated to at least one SLC (active) and the compounds with no associations (inactive) to the DrugBank dataset (Fig. 5d, Supplementary Fig. 5b) as well as between them (Supplementary Fig. 5c) and again observed no trend that would suggest a presence of specific properties in the set of drugs showing associations with SLCs.

Discussion

Transmembrane transporters represent a major class of metabolic genes involved in several cellular processes affecting drug potency and activity, including the uptake and extrusion of these xenobiotic compounds as well as all kinds of biologically active molecules[2]. Members of the ABCs and SLCs transporter families have been increasingly recognized as key players in determining distribution and availability of drugs, especially in liver, kidney, intestine and inter-organ interfaces such as the blood-brain barrier[1]. In the past, the discovery of specific transporters for several cytotoxic compounds by insertional mutagenesis and CRISPR/Cas9-based screens provided clear examples of the power of genetic approaches for the identification of such relationships[17–19,41]. However, despite the unambiguous involvement of these transporters in drug uptake, it is possible that these relationships are exceptional in nature and confined to particular chemical subtypes. As an alternative possibility, most drugs thought to act on an intracellular target would indeed require a membrane-spanning transporter to gain access to the inside of cells, the lack of convenient genetic tools in cellular intact systems having impeded their systematic identification. As motivation for this study, we therefore reasoned that a focused forward genetic approach in live human cells (Fig. 1a, Supplementary Table 1) would allow us to systematically investigate the frequency by which a drug or drug-like compound would be affected by the function of an SLC gene.

As read-out compatible with genetic screening, we opted for simple cellular survival, as it allows to monitor strong selective pressures and to focus on cytotoxic/cytostatic compounds of clinical relevance. A cheminformatics analysis of the set of 60 screened compounds, which included several approved drugs (Fig. 5, Supplementary Table 2), showed no bias in physicochemical properties compared to the DrugBank database, thus supporting its use as a set representative of the chemical space occupied by drugs.

Antimetabolites such as folate- and nucleoside-analogs scored strongly in our setting, recapitulating the known cases of drug uptake mediated by transporters such as SLC19A1 and SLC29A1 (Fig. 2c, 3b, 4b). Resistance to such compounds through mutations or altered expression levels in these transporters have been previously reported[42,43], suggesting that our results provide insight into potential resistance mechanisms to cytotoxic compounds. Interestingly, we also identified several additional strong interactions across different drug classes, such as the role of the iron transporter SLC11A2 in determining resistance to artemisinin derivatives (Fig. 2c, 3b). This is consistent with the positive correlation between intracellular iron levels and drug cytotoxicity previously suggested for these compounds[44]. We also validated interactions between artesunate/dihydroartemisinin and the monocarboxylate transporter SLC16A1, showing that SLC16A1 protein levels determine the sensitivity to artesunate (Fig. 4c-d), as well as between cisplatin and the transporters SLC35A2 and SLC38A5 (Fig. 2c, 3b). The latter is particularly interesting as SLC38A5 is a

glutamine transporter expressed at high levels in cells of hematopoietic origin and several studies reported a dependence on glutaminolysis for cisplatin-resistant cells[45,46]. As we did not observe compensating upregulation of glutamine transporters upon SLC38A5 loss (Supplementary Fig. 4a), it is therefore possible that loss of this transporter impacts other pathways important for cisplatin-induced cytotoxicity, such as autophagy, as reported for the related family member SLC38A1[47]. We observed several interactions comprising key, often essential, transporters involved in major energetic pathways such as SLC2A1/GLUT1, the major glucose transporter at the plasma membrane, SLC25A3, the mitochondrial phosphate/copper transporter, or MTCH2, a mitochondrial carrier involved in apoptosis regulation and a repressor of mitochondrial metabolism (Fig. 2c, 3b). It has been shown that resistance to cytotoxic drugs often requires major metabolic rearrangements: e.g. glutaminolysis and cisplatin resistance[45,46], a switch to oxidative phosphorylation in cytarabine resistance[48] or drug-specific dependence on glycolysis[49]. The fact that several of the SLC-drug associations identified involve SLCs important for cellular fitness therefore speaks to the strong metabolic pressure a cytotoxic drug imposes on a target cell.

As much as 80% (47/60) of the small chemical molecules tested were functionally dependent on an SLC gene (Fig. 2c). The large number and proportion of novel drug-SLC relationships identified here strongly argues for a more general role of transporters than currently appreciated in the uptake and activity of drugs into target tissues. Previous surveys of cytotoxic compounds in yeast showed that transporter deletion affected the activity and uptake of ~70% of the compounds tested (18/26), a proportion remarkably similar to the one observed in this study[50]. In light of the outcome of these systematic functional surveys, the notion that membrane permeability and bioavailability of drugs primarily reside in their ability to diffuse across membranes may therefore require revision. As for the remaining 20% of compounds that did not show an association with SLCs, we did not observe any striking difference in their chemical properties when compared to the SLC-associated ones (Fig. 5d), suggesting that these molecules may exert their activity or access cells through SLCs with redundant function (i.e. multiple SLCs for a given substrate). In these scenarios, genetic depletion of a single SLC would not be sufficient to score in our experimental set-up and higher-order genetic perturbations, of the type that could be achieved with vectors bearing multiple sgRNAs, may be required. It is also possible that proteins other than SLCs are involved in drug uptake, such as yet poorly characterized TMEM proteins, ion channels or entirely uncharacterized proteins. Larger, ideally combinatorial, focused or genome-wide CRISPR/Cas9 screens are therefore likely to reveal the involvement of additional proteins exerting drug-transporting function. In any case, it is now feasible and urgent to investigate the genetic determinants of drug activity and especially uptake. The evidence provided here is clearly beyond anecdotal and will hopefully trigger further campaigns of similar scope. Knowledge of the transporters affecting uptake and activity of drugs in tumors and tissues is certain to represent a cornerstone of precision therapies of the future and allow us to predict and counteract resistance mechanisms. Moreover, the relationship between the expression of SLCs, cellular/organismal metabolism and nutrition is likely to allow the opening of novel therapeutic avenues.

Methods

Generation of an SLC-wide CRISPR/Cas9 lentiviral library

A set of single guide RNAs (sgRNAs) targeting 388 human SLC genes, generally with six sgRNAs per gene, were manually selected (or generated) to include sequences with predicted high efficiency and specificity, as assessed in Doench *et al*[51], and to minimize targeting of other SLCs or of ABC transporters (Supplementary Table 1). sgRNAs targeting six SLC pseudogenes (SLC7A5P1, SLC7A5P2, SLC9A7P1, SLC2A3P1, SLC25AP5, SLC35E1P1) for which transcription was previously reported in at least two expression datasets (FANTOM5, CCLE, ENCODE, Cosmic, GENCODE, Uhlen et al, Illumina)[52] were also included. An additional set of 120 sgRNAs targeting 20 genes essential in both KBM7 and HAP1 cells[53] based on the number of retroviral insertions observed were also selected (Supplementary Table 1). Finally, a set of 120 non-targeting sgRNAs was included by generating random 20-mers and selecting for sequences with at least three (for the strong PAM NGG) or two (for the PAM NAG) mismatches from any genomic sequence with E-CRISP Evaluation[54] Adapter sequences were added to the 5' and 3' sequences (5'prefix: TGGAAAGGACGAAACACCG, 3'suffix: GTTTTAGAGCTAGAAATAGCAAGTTAAAATAAGGC) to allow cloning by Gibson assembly in the lentiCRISPRv2 vector (Addgene #52961). The oligos were synthetized as a pool by LC Sciences. Full-length oligonucleotides (74 nt) were amplified by PCR using Phusion HS Flex (NEB) and size-selected using a 2% agarose gel (Primers: SLC_ArrayF TAACTTGAAAGTATTTCGATTTCTTGGCTTTATATATCTTGTGGAAAGGAC GAAACACCG, SLC_ArrayR ACTTTTTCAAGTTGATAACGGACTAGCCTTATTTTAACTTGCTATTTCT AGCTCTAAAAC) The vector was digested with BsmBI (NEB) for 1h at 55˚C, heat inactivated for 20' at 80˚C, following by incubation with Antarctic phosphatase (NEB) for 30' at 37˚C. A 10 μl Gibson ligation reaction (NEB) was performed using 5 ng of the gel-purified inserts and 12.5 ng of the vector, incubated for 1h at 50˚C and dialyzed against water for 30' at RT. The reaction was then transformed in Lucigen Endura cells and plated on two 245mm plates. Colonies (equivalent to approximately 200X coverage) were grown at 32˚C for 16-20h hours and then scraped from the plates. The plasmid was purified with the Endo-Free Mega prep kit (Qiagen).

Library NGS sequencing

Initial amplification of the library for NGS sequencing was performed by a two-step PCR protocol as described in Sanjana *et al*[55]. Due to the presence of unspecific bands affecting the quality of the sequencing experiments, later samples were processed with a single-step PCR derived from Konermann *et al*[56]. The PCR primers used to add barcodes and Illumina adapters were modified to allow for double indexing of samples.

Enrichment analysis

sgRNA sequences were extracted from NGS reads, matched against the original sgRNA library index and counted using an in-house python script. Samples with less than 10^5 total reads were excluded from further analysis. A two-step approach was implemented in order to obtain a final list of enriched candidate genes. First, differential abundance of individual

sgRNAs was estimated using DESeq2 v1.20. Models accounted for both treatment and time variables when time 0 samples were available; otherwise only the treatment factor was considered. Contrasts were performed individually for each treatment and dose vs controls (DMSO and untreated), and significance was tested using either one- or two-tailed Wald tests (i.e. alternative hypothesis LFC>0 for enrichment, and abs(LFC)>0 for enrichment or depletion, respectively). Then, sgRNAs were sorted by log2 fold change and aggregated into genes using Gene Set Enrichment Analysis (fgsea R package v1.7). To avoid false positives, only significant sgRNAs (p-value ≥ 0.05) were considered for enrichment, requiring also a minimum of two sgRNAs per gene. Gene enrichment significance was estimated by a permutation test using 10^8 permutations, and p-values were corrected for multiple testing using the Benjamini-Hochberg procedure (FDR).

Cell lines

HAP1 cells (Horizon Genomics) were grown in IMDM media (Gibco) supplemented with 10% FCS (Gibco) and 1% penicillin/streptomycin. For screening purposes, haploid cells were selected by FACS sorting after staining with Vybrant DyeCycle Ruby stain (Thermo Fisher Scientific), expanded for 3-5 days and frozen until further use. For CRISPR-based knockout cell lines, sgRNAs were designed using CHOPCHOP[57] and cloned into pLentiCRISPRv2 (Addgene, #52961), LGPIG (pLentiGuide-PuroR-IRES-GFP) or LGPIC (pLentiGuide-PuroR-IRES-mCherry)[58]. sgRen targeting Renilla luciferase cDNA was used as negative control sgRNA[58]. Editing efficiency was determined with Tide-seq[59]. The SLC-deficient clones (ΔSLC16A1_2882-2, renamed as ΔSLC16A1_2 in the text, and clone ΔSLC16A1_2882-10, renamed as ΔSLC16A1_1; ΔSLC19A1_1771-2, ΔSLC19A1_1771-12 renamed as ΔSLC19A1_1 and ΔSLC19A1_2 respectively; ΔSLC38A5_CRISPR_ 1691-11 renamed as ΔSLC38A5; ΔSLC11A2_1897-11 renamed as ΔSLC11A2) were purchased from Horizon Genomics or available in-house[60]. Codon-optimized SLC16A1 cDNA or eGFP cDNA sequences were obtained from the ReSOLUTE consortium (www.re-solute.eu) and cloned in the pLX304 vector (Addgene plasmid #25890).

Drug cytotoxicity screens

To mimic the genetic screen conditions, HAP1 cells were infected with a lentiCRISPRv2 vector carrying an sgRNA targeting the *Renilla* luciferase gene and selected with puromycin selection (1μg/ml) for 7 days. WT and lenti-infected cells were screened against a library composed of 1812 compounds at a single concentration in the range of 10-50μM. All screened compounds were obtained from commercial sources. Viability was measured by CellTiterGlo assay (Promega) after 72h of treatment. DMSO and Digitoxin were used as negative and positive controls, respectively, to calculate cytotoxicity. Hits were defined as compounds giving more than 50% inhibition compared to DMSO controls. 8-point dose-response curves were performed to determine the IC_{50} values of the cytotoxic compounds in lentivirus-infected HAP1 cells.

Chemical space analysis

Data curation was performed using a KNIME 3.6.0 workflow which incorporates the python packages RDKit 2018.09.01 and MolVS 0.1.1 for handling and standardizing molecules (python 3.6.6 was used). First, all compounds were neutralized by adding or removing

protons. Then, compounds were cleaned by standardizing the representation of all aromatic rings, double bonds, hydrogens, tautomers and mesomers. Thereafter, all salts and mixtures were removed. In order to remove duplicates InChIKeys were calculated and all compounds were aggregated according to these InChIKeys. Chiral centers were also removed, as this stereochemistry information is often incorrectly assigned, which can lead to a lower detection rate of duplicates. Furthermore, only 2D descriptors were calculated, which cannot differentiate between enantiomers or diastereomers. It is noteworthy that the calculated 2D descriptors cannot be used to describe inorganic compounds, therefore those compounds were removed from further analysis. All 22 descriptors were computed with the RDKit nodes available in KNIME 3.6.0. Data visualization was performed in Rstudio 1.1.463 with R 3.4.4. Bar plots and violin plots were computed with ggplot2 3.1.0, the correlation of descriptors plot was computed with corrplot 0.84. Principal components analysis (PCA) was performed with the R packages factoextra and FactoMineR.

Genetic screens

Viral particles were generated by transient transfection of low passage, subconfluent HEK293T cells with the SLC-targeting library and packaging plasmids psPAX2 (Addgene #12260), pMD2.G (Addgene #12259) using PolyFect (Qiagen). After 24h the media was changed to fresh IMDM media supplemented with 10% FCS and antibiotics. The viral supernatant was collected after 48h, filtered and stored at -80° C until further use. The supernatant dilution, necessary to infect haploid HAP1 cells at an MOI (multiplicity of infection) of 0.2-0.3, was determined by puromycin survival after transduction. HAP1 cells were infected in duplicates with the SLC KO library at high coverage (1000x) and after selection for 7 days with puromycin (1μg/ml) an initial sample was collected to control for library composition. Cells were then treated with multiple concentrations (generally 1X, 3X or 10X the IC_{50}) of the cytotoxic compounds or vehicle (DMSO or DMF) controls for 72h and, when surviving cells were present, cell samples collected from both treated and control samples.

Multicolor competition assay

Flow cytometry-based multi-color competition assays (MCA) were performed as described previously[8]. Briefly, HAP1 cells expressing LGPIC-sgRen (mCherry-positive) were mixed in 1:1 ratio with LGPIG (eGFP-positive) reporter cells containing sgRNAs targeting the gene of interest. The mixed cell populations were incubated with vehicle or drug for up to 10 days. The respective percentage of viable (FSC/SSC) mCherry-positive and eGFP-positive cells at the indicated time points was quantified by flow cytometry. Samples were analyzed on an LSR Fortessa (BD Biosciences) and data analysis was performed using FlowJo software (Tree Star Inc., USA). Individual ratios were normalized to day 0 controls and then log transformed. In order to detect significant changes upon treatment, a two-way ANOVA model with treatment and KO factors was fitted for every gene and day using biological replicates only (average of three technical replicates) and then a one-tailed Dunnett’s test was performed to compare each treatment vs the control (DMSO for all drugs but cisplatin, DMF for cisplatin).

Viability assays

For viability assays, 10.000 HAP1 cells/well were plated in a 96-well plate and a 10-step, 3-fold dilution series performed in triplicates. Viability was measured by CellTiterGlo assay (Promega) after 72h of treatment.

Liquid chromatography tandem mass spectrometry (LC-MS/MS) assay

Uptake assays were performed by plating HAP1 cells in 6-well ($8x10^5$ cells/well) or 10cm dishes ($4x10^6$ cells/plates) the day prior to the experiment. Cells were treated with 2μM (methotrexate) or 20μM (artesunate) for 1h at 37°C. Cells were then washed two times with ice-cold TBS and lysed in 100-1000μL of 80% ice -cold methanol. After centrifugation at 4°C, 16,000g for 20 minutes, supernatants were dried with a nitrogen evaporator and reconstituted in 50μL methanol. The concentrated samples were analyzed by LC -MS/MS (Waters Acquity UHPLC system coupled to Waters XevoTQMS mass spectrometer).

The chromatographic separations were carried on an ACQUITY UHPLC HSS T3, 1.8μm, 2.1x100mm analytical column (Waters) equipped with a VanGuard: HSS T3, 2.1x5mm pre-column (Waters). The column was maintained at a temperature of 40°C and 2μL sample were injected per run. Mobile phase A was 0.1% (v/v) formic acid in water and mobile phase B was 0.1% (v/v) formic acid in methanol. For the analysis of methotrexate, a gradient elution was applied by increasing mobile phase B from 5% to 95% within 7 minutes, total analysis time was 10min with the flow rate set to 0.5mL/min. The compounds were detected in a positive electrospray ionization mode with the following settings: capillary voltage: 3.2kV, cone voltage: 30 V, source temperature: 150°C. The multiple reaction monitoring transition: 454.94 -> 134 with collision energy of 20V was used for methotrexate. For the analysis of artesunate, a gradient elution was applied by increasing mobile phase B (0.1% (v/v) formic acid in acetonitrile) from 40% to 95% within 3.1min, total analysis time was 4 min with the flow rate set to 0.5mL/min. Using the same mass spectrometry settings described above, the multiple reaction monitoring transition 407 -> 261 with collision energy of 17V was used to detect artesunate. A five-point calibration curve was determined to allow quantification of the compounds. Data analysis was performed using the MassLynx V4.1 (Waters) software.

Gene expression analysis (RNA-Seq)

HAP1 cells were plated ($2×10^6$ cells per condition, in triplicate) the day before and then treated with either artesunate (1.8μM), cisplatin (1μM) or the corresponding vehicles (DMSO or DMF) for 24h. Cells were harvested and RNA was isolated using the QIAGEN RNeasy Mini kit including a DNase I digest step. RNA-Seq libraries were prepared using QuantSeq 3’ mRNA-Seq Library Prep Kit FWD for Illumina (Lexogen) according to the manufacture’s protocol. The libraries were sequenced by the Biomedical Sequencing Facility at CeMM using the Illumina HiSeq 4000 platform at the 50 bp single-end configuration. Raw sequencing reads were demultiplexed, and after barcode, adaptor and quality trimming with cutadapt (https://cutadapt.readthedocs.io/en/stable/), quality control was performed using FastQC (http://www.bioinformatics.babraham.ac.uk/projects/fastqc/). The remaining reads were mapped to the GRCh38/h38 human genome assembly using genomic short-read RNA-Seq aligner STAR version 2.5. We obtained more than 98%

mapped reads in each sample with 60 – 80% of reads mapping to unique genomic location. Transcripts were quantified using End Sequence Analysis Toolkit (ESAT). Differential expression analysis was performed using independent triplicates with DESeq2 (1.21.21) on the basis of read counts. Exploratory data analysis and visualizations were performed in R-project version 3.4.2 (Foundation for Statistical Computing, Vienna, Austria, https://www.R-project.org/) with Rstudio IDE version 1.0.143, ggplot2 (3.0.0), dplyr (0.7.6), readr (1.1.1), gplots (3.0.1).

Transcription factor targets enrichment test

Regulatory networks obtained from TRRUST version 2. Transcription factor targets enrichment analysis was performed using Fisher's exact test and p-values were corrected for multiple testing using the Benjamini-Hochberg procedure (FDR).

Confocal imaging

For the confocal imaging of 293T cells, high precision microscope cover glasses (Marienfeld) were coated with poly-L-lysine hydrobromide (p6282, Sigma-Aldrich) according to the manufacturer's protocol. Cells were seeded onto cover glasses in normal growth medium and fixed in 4% Formaldehyde solution (AppliChem) in PBS 1x after 24h of incubation. Permeabilization and blocking of samples was performed in blocking solution (10% FCS, 0.3% Saponin (47036, Sigma-Aldrich) in PBS 1x) for 1h rocking. Anti-V5 Tag primary antibody (Thermo Fischer Scientific, #46-0705) was diluted 1:500 in blocking solution and applied for 2h at room temperature, rocking. Samples were washed three times in blocking solution and anti-mouse Alexa Fluor 594 (Thermo Fischer Scientific, #A-11005) was applied 1:400 in blocking solution for 1h at room temperature, rocking. After three times washing in blocking solution nuclei were counterstained with DAPI 1:1000 in PBS 1x, for 10min, rocking. Cover glasses were mounted onto microscopy slides using ProLong Gold (Thermo Fischer Scientific) antifade mountant. Image acquisition was performed on a confocal laser scanning microscope (Zeiss LSM 780, Carl Zeiss AG), equipped with an Airyscan detector using ZEN black 2.3 (Carl Zeiss AG).

Supplementary Material

Refer to Web version on PubMed Central for supplementary material.

Acknowledgments

We thank all members of the Superti-Furga laboratory for discussions and feedback. We are also grateful to the Biomedical Sequencing facility for advice on Illumina sequencing and to the Flow Cytometry Core Facility of the Vienna Medical University for help with FACS sorting. We further thank Dr. Bojan Vilagos for graphical input and advice and Sara Sdelci for scientific discussions and insight. We acknowledge support by the Austrian Academy of Sciences, the European Research Council (ERC AdG 695214 GameofGates, E.G., G.F.), Austrian Science Fund (FWF I2192-B22 ERASE, A.C-R; FWF P29250-B30 VITRA, E.G, J.K, G.F,) and by a Marie Sklodowska-Curie fellowship to E.G. (MSCA-IF-2014-661491). Research in the Kubicek laboratory is supported by the Austrian Federal Ministry for Digital and Economic Affairs and the National Foundation for Research, Technology, and Development, the Austrian Science Fund (FWF) F4701 and the European Research Council (ERC) under the European Union's Horizon 2020 research and innovation programme (ERC-CoG-772437). The Pharmacoinformatics Research Group (Ecker lab) acknowledges funding provided by the Austrian Science Fund FWF AW012321 MolTag.

Europe PMC Funders Author Manuscripts

Data Availability Statement

The data and code that support the findings of this study are available on request from the corresponding author G.S-F. Source data for figures 2 and 3 are provided with the paper.

References

1. Gonzalez, FJ, Coughtrie, M, Tukey, RH. Drug MetabolismGoodman & Gilman's: The Pharmacological Basis of Therapeutics. Brunton, LL, Chabner, BA, Knollmann, BC, editors. McGraw-Hill Education; 2015.
2. Nigam SK. What do drug transporters really do? Nat Rev Drug Discov. 2014; 14:29–44. [PubMed: 25475361]
3. César-Razquin A, et al. A Call for Systematic Research on Solute Carriers. Cell. 2015; 162:478–487. [PubMed: 26232220]
4. Fletcher JI, Haber M, Henderson MJ, Norris MD. ABC transporters in cancer: more than just drug efflux pumps. Nat Rev Cancer. 2010; 10:147–156. [PubMed: 20075923]
5. Hediger MA, Clémençon B, Burrier RE, Bruford EA. The ABCs of membrane transporters in health and disease (SLC series): Introduction. Mol Aspects Med. 2013; 34:95–107. [PubMed: 23506860]
6. Motohashi H, Inui K. Multidrug and toxin extrusion family SLC47: Physiological, pharmacokinetic and toxicokinetic importance of MATE1 and MATE2-K. Mol Aspects Med. 2013; 34:661–668. [PubMed: 23506899]
7. Estudante M, Soveral G, Morais JG, Benet LZ. Insights into solute carriers: physiological functions and implications in disease and pharmacokinetics. MedChemComm. 2016; 7:1462–1478.
8. Geier EG, et al. Profiling Solute Carrier Transporters in the Human Blood-Brain Barrier. Clin Pharmacol Ther. 2013; 94:636–639. [PubMed: 24013810]
9. Giacomini KM, et al. International Transporter Consortium Commentary on Clinically Important Transporter Polymorphisms. Clin Pharmacol Ther. 2013; 94:23–26. [PubMed: 23778707]
10. U.S. Department of Health and Human Services Food and Drug Administration Center for Drug Evaluation and Research (CDER). Clinical Drug Interaction Studies — Study Design, Data Analysis, and Clinical Implications. 2017
11. Matsson P, et al. Quantifying the impact of transporters on cellular drug permeability. Trends Pharmacol Sci. 2015; 36:255–262. [PubMed: 25799456]
12. Dobson PD, Kell DB. Carrier-mediated cellular uptake of pharmaceutical drugs: an exception or the rule? Nat Rev Drug Discov. 2008; 7:205–220. [PubMed: 18309312]
13. Sugano K, et al. Coexistence of passive and carrier-mediated processes in drug transport. Nat Rev Drug Discov. 2010; 9:597–614. [PubMed: 20671764]
14. Young JD, Yao SYM, Baldwin JM, Cass CE, Baldwin SA. The human concentrative and equilibrative nucleoside transporter families, SLC28 and SLC29. Mol Aspects Med. 2013; 34:529–547. [PubMed: 23506887]
15. Icard P, et al. How the Warburg effect supports aggressiveness and drug resistance of cancer cells? Drug Resist Updat. 2018; 38:1–11. [PubMed: 29857814]
16. Reczek CR, et al. A CRISPR screen identifies a pathway required for paraquat-induced cell death. Nat Chem Biol. 2017; 13:1274–1279. [PubMed: 29058724]
17. Winter GE, et al. The solute carrier SLC35F2 enables YM155-mediated DNA damage toxicity. Nat Chem Biol. 2014; 10:768–773. [PubMed: 25064833]
18. Birsoy K, et al. MCT1-mediated transport of a toxic molecule is an effective strategy for targeting glycolytic tumors. Nat Genet. 2012; 45:104–108. [PubMed: 23202129]
19. Reiling JH, et al. A haploid genetic screen identifies the major facilitator domain containing 2A (MFSD2A) transporter as a key mediator in the response to tunicamycin. Proc Natl Acad Sci. 2011; 108:11756–11765. [PubMed: 21677192]
20. Blomen VA, et al. Gene essentiality and synthetic lethality in haploid human cells. Science. 2015; 350:1092–6. [PubMed: 26472760]

21. Klein M-C, et al. AXER is an ATP/ADP exchanger in the membrane of the endoplasmic reticulum. Nat Commun. 2018; 9:3489. [PubMed: 30154480]
22. Robinson AJ, Kunji ERS, Gross A. Mitochondrial carrier homolog 2 (MTCH2): The recruitment and evolution of a mitochondrial carrier protein to a critical player in apoptosis. Exp Cell Res. 2012; 318:1316–1323. [PubMed: 22326460]
23. O'Hagan S, Wright Muelas M, Day PJ, Lundberg E, Kell DB. GeneGini: Assessment via the Gini Coefficient of Reference "Housekeeping" Genes and Diverse Human Transporter Expression Profiles. Cell Syst. 2018; 6:230–244. [PubMed: 29428416]
24. César-Razquin A, et al. In silico Prioritization of Transporter-Drug Relationships From Drug Sensitivity Screens. Front Pharmacol. 2018; 9:1011. [PubMed: 30245630]
25. Licciardello MP, et al. A combinatorial screen of the CLOUD uncovers a synergy targeting the androgen receptor. Nat Chem Biol. 2017; 13:771–778. [PubMed: 28530711]
26. Zhao R, Diop-Bove N, Visentin M, Goldman ID. Mechanisms of Membrane Transport of Folates into Cells and Across Epithelia. Annu Rev Nutr. 2011; 31:177–201. [PubMed: 21568705]
27. Sirotnak FM, DeGraw JI, Moccio DM, Samuels LL, Goutas LJ. New folate analogs of the 10-deaza-aminopterin series Basis for structural design and biochemical and pharmacologic properties. Cancer Chemother Pharmacol. 1984; 12:18–25. [PubMed: 6690069]
28. Waalkes TP, Makulu DR. Pharmacologic aspects of pentamidine. Natl Cancer Inst Monogr. 1976; 43:171–177. [PubMed: 1018718]
29. Grottker J, Rosenberger A, Burckhardt G, Hagos Y. Interaction of human multidrug and toxin extrusion 1 (MATE1) transporter with antineoplastic agents. Drug Metabol Drug Interact. 2011; 26
30. Yang N-D, et al. Artesunate Induces Cell Death in Human Cancer Cells via Enhancing Lysosomal Function and Lysosomal Degradation of Ferritin. J Biol Chem. 2014; 289:33425–33441. [PubMed: 25305013]
31. Cui L, Su X. Discovery, mechanisms of action and combination therapy of artemisinin. Expert Rev Anti Infect Ther. 2009; 7:999–1013. [PubMed: 19803708]
32. Montalbetti N, Simonin A, Kovacs G, Hediger MA. Mammalian iron transporters: Families SLC11 and SLC40. Mol Aspects Med. 2013; 34:270–287. [PubMed: 23506870]
33. Kell DB. Iron behaving badly: inappropriate iron chelation as a major contributor to the aetiology of vascular and other progressive inflammatory and degenerative diseases. BMC Med Genomics. 2009; 2:2. [PubMed: 19133145]
34. Pérez-Escuredo J, et al. Monocarboxylate transporters in the brain and in cancer. Biochim Biophys Acta BBA - Mol Cell Res. 2016; 1863:2481–2497.
35. Song Z. Roles of the nucleotide sugar transporters (SLC35 family) in health and disease. Mol Aspects Med. 2013; 34:590–600. [PubMed: 23506892]
36. Schiöth HB, Roshanbin S, Hägglund MGA, Fredriksson R. Evolutionary origin of amino acid transporter families SLC32, SLC36 and SLC38 and physiological, pathological and therapeutic aspects. Mol Aspects Med. 2013; 34:571–585. [PubMed: 23506890]
37. Våtsveen TK, et al. Artesunate shows potent anti-tumor activity in B-cell lymphoma. J Hematol OncolJ Hematol Oncol. 2018; 11:23. [PubMed: 29458389]
38. Wang N, Zeng G-Z, Yin J-L, Bian Z-X. Artesunate activates the ATF4-CHOP-CHAC1 pathway and affects ferroptosis in Burkitt's Lymphoma. Biochem Biophys Res Commun. 2019; 519:533–539. [PubMed: 31537387]
39. St Germain C, et al. Cisplatin induces cytotoxicity through the mitogen-activated protein kinase pathways and activating transcription factor 3. Neoplasia N Y N. 2010; 12:527–538.
40. Wishart DS, et al. DrugBank 5.0: a major update to the DrugBank database for 2018. Nucleic Acids Res. 2017; 46:D1074–D1082.
41. Yu Z, et al. Identification of a transporter complex responsible for the cytosolic entry of nitrogen-containing bisphosphonates. eLife. 2018; 7 e36620 [PubMed: 29745899]
42. Yee SW, et al. SLC19A1 Pharmacogenomics Summary. Pharmacogenet Genomics. 2010; 20:708–715. [PubMed: 20811316]
43. Pastor-Anglada M, Pérez-Torras S. Nucleoside transporter proteins as biomarkers of drug responsiveness and drug targets. Front Pharmacol. 2015; 6:13. [PubMed: 25713533]

44. Lai H, Singh NP. Selective cancer cell cytotoxicity from exposure to dihydroartemisinin and holotransferrin. Cancer Lett. 1995; 91:41–46. [PubMed: 7750093]
45. Duan G, et al. Increased Glutamine Consumption in Cisplatin-Resistant Cells Has a Negative Impact on Cell Growth. Sci Rep. 2018; 8:4067. [PubMed: 29511244]
46. Guidi N, Longo VD. Periodic fasting starves cisplatin-resistant cancers to death. EMBO J. 2018; 37 e99815 [PubMed: 29875131]
47. Yamada D, et al. Inhibition of the glutamine transporter SNAT1 confers neuroprotection in mice by modulating the mTOR-autophagy system. Commun Biol. 2019; 2:1–11. [PubMed: 30740537]
48. Farge T, et al. Chemotherapy-Resistant Human Acute Myeloid Leukemia Cells Are Not Enriched for Leukemic Stem Cells but Require Oxidative Metabolism. Cancer Discov. 2017; 7:716–735. [PubMed: 28416471]
49. Bhattacharya B, Mohd Omar MF, Soong R. The Warburg effect and drug resistance: The Warburg effect and drug resistance. Br J Pharmacol. 2016; 173:970–979. [PubMed: 26750865]
50. Lanthaler K, et al. Genome-wide assessment of the carriers involved in the cellular uptake of drugs: a model system in yeast. BMC Biol. 2011; 9:70. [PubMed: 22023736]
51. Doench JG, et al. Rational design of highly active sgRNAs for CRISPR-Cas9-mediated gene inactivation. Nature Biotechnology. 2014; 32:1262–1267.
52. Uhlén M, et al. Tissue-based map of the human proteome. Science. 2015; 347 1260419 [PubMed: 25613900]
53. Blomen VA, et al. Gene essentiality and synthetic lethality in haploid human cells. Science. 2015; 350:1092–6. [PubMed: 26472760]
54. Heigwer F, Kerr G, Boutros M. E-CRISP: fast CRISPR target site identification. Nature methods. 2014; 11:122–123. [PubMed: 24481216]
55. Sanjana NE, Shalem O, Zhang F. Improved vectors and genome-wide libraries for CRISPR screening. Nature methods. 2014; 11:783–784. [PubMed: 25075903]
56. Konermann S, et al. Genome-scale transcriptional activation by an engineered CRISPR-Cas9 complex. Nature. 2014; 517:583–8. [PubMed: 25494202]
57. Montague TG, Cruz JM, Gagnon JA, Church GM, Valen E. CHOPCHOP: a CRISPR/Cas9 and TALEN web tool for genome editing. Nucleic Acids Research. 2014; 42:W401–W407. [PubMed: 24861617]
58. Bigenzahn JW, et al. LZTR1 is a regulator of RAS ubiquitination and signaling. Science. 2018; 362:1171–1177. [PubMed: 30442766]
59. Brinkman EK, Chen T, Amendola M, van Steensel B. Easy quantitative assessment of genome editing by sequence trace decomposition. Nucleic Acids Research. 2014; 42 e168 [PubMed: 25300484]
60. Moskovskich A, et al. The transporters SLC35A1 and SLC30A1 play opposite roles in cell survival upon VSV virus infection. Sci Rep. 2019; 9:10471. [PubMed: 31320712]

Europe PMC Funders Author Manuscripts

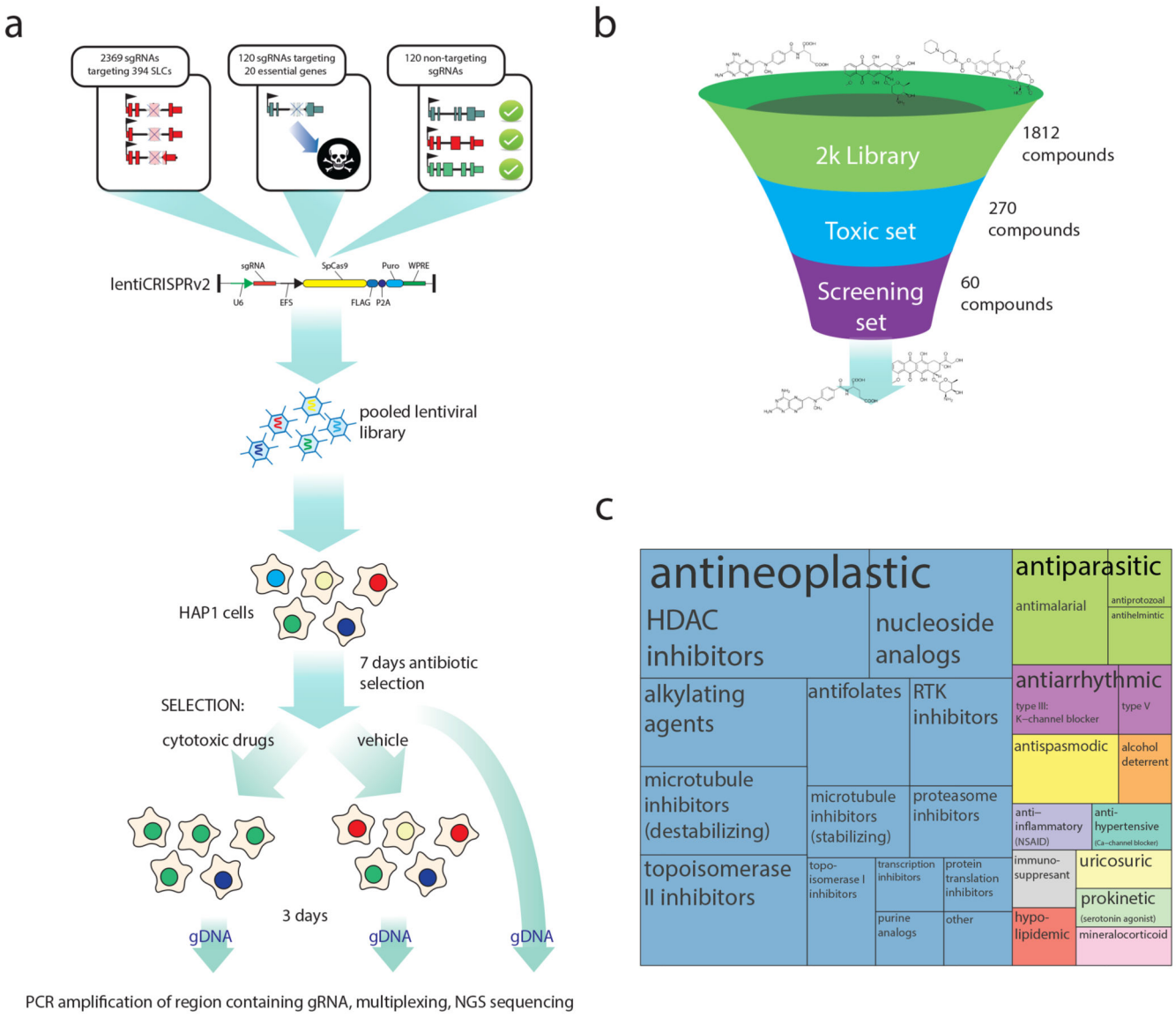

Figure 1.

a. Schematic view of the composition of the SLC-focused CRISPR/Cas9 library and experimental outline of the genetic screen. **b**. Schematic view of the compound sets used in this study and the sequential filtering steps applied to the selection of a final set of 60 drugs for screening. **c**. Treeplot view of the drug classes and subclasses included in the screening set.

Europe PMC Funders Author Manuscripts

Europe PMC Funders Author Manuscripts

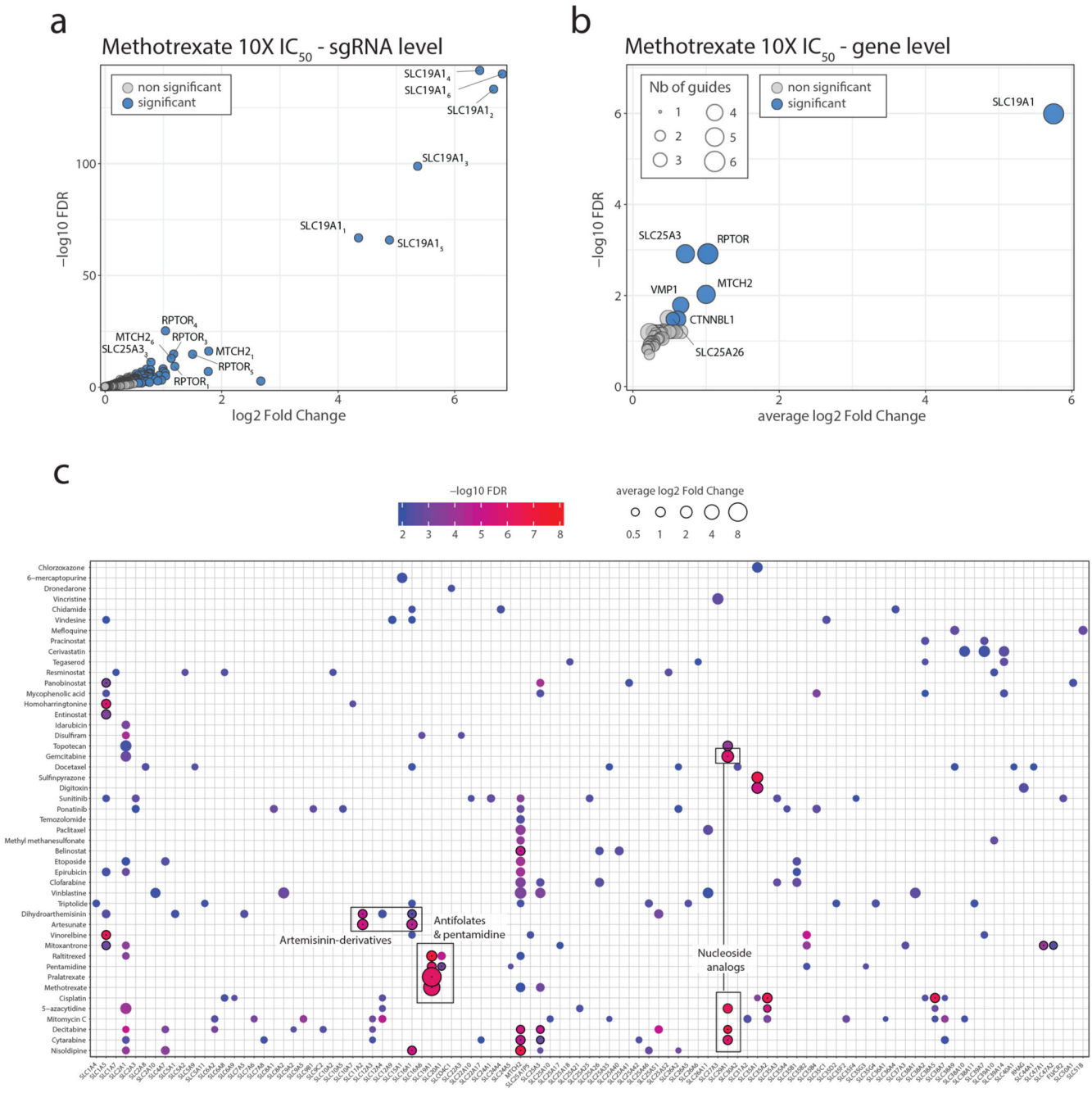

Figure 2.

a. sgRNA-level enrichment for samples treated with 10X IC_{50} methotrexate, as determined by DESeq2. All six sgRNAs targeting the SLC19A1 gene showed significant enrichment (n=2). **b**. Gene-level enrichment for samples treated with 10X IC_{50} methotrexate, as determined by GSEA. Average log2 fold change for the significant sgRNAs for each gene is shown in the x-axis. Circle size indicates the number of significant sgRNAs. (n=2). **c**. Overview of significantly enriched SLCs (FDR≤1%) identified upon treatment with different compounds. Significant enrichments for all different doses of the same compound are

merged together (union), selecting the most significant value in the case of repeated hits. SLC genes are ordered by name, and treatments are ordered by hierarchical clustering based on the gene-level results. Associations that underwent validation by MCA are shown with a black edge, and successfully validated cases are represented with a black dot in the center. All results are derived by pooling data from at least two independent experiments (n=2-3).

Europe PMC Funders Author Manuscripts

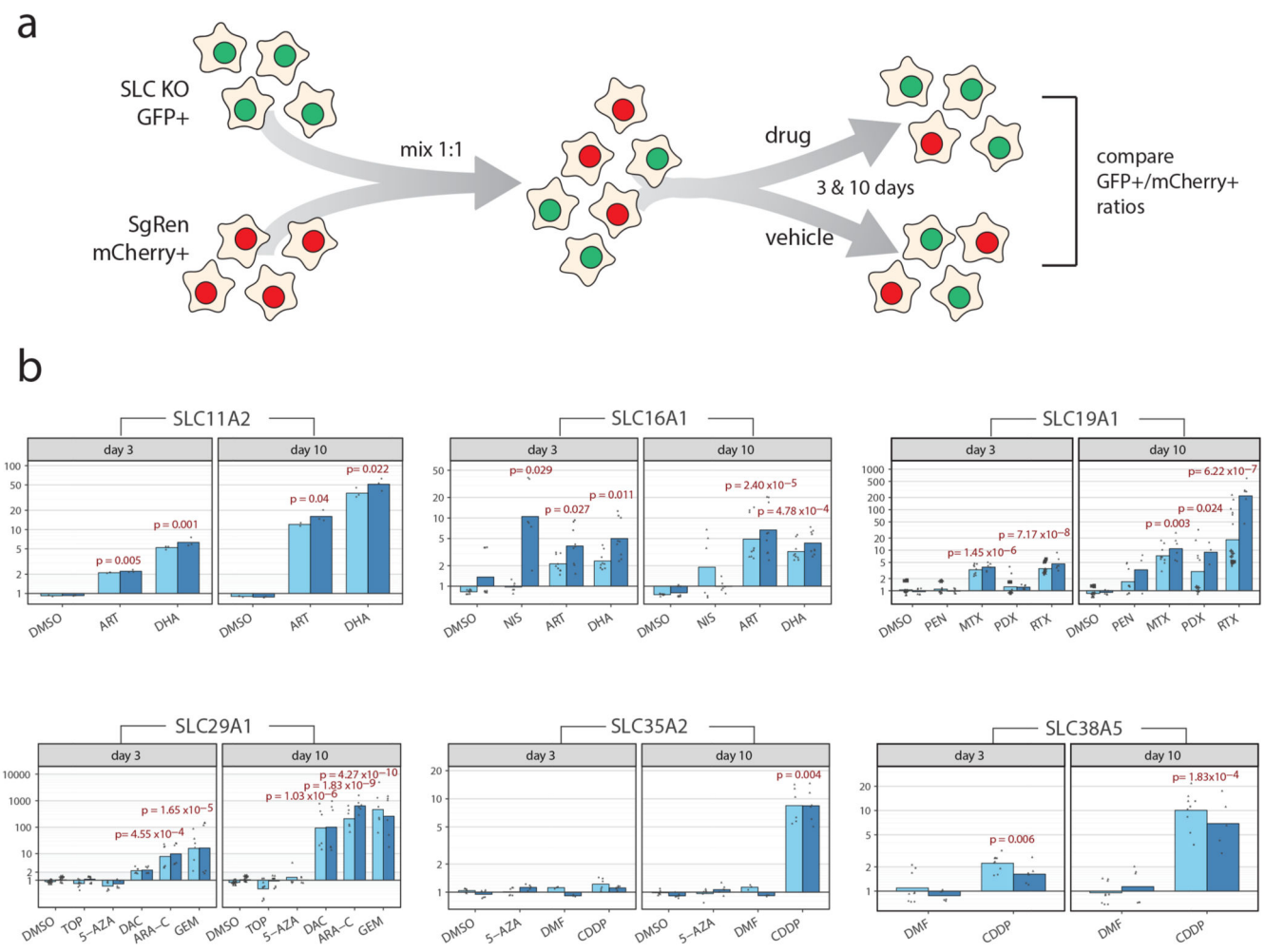

Figure 3.

a. Schematic view of the Multicolor Competition Assay (MCA). **b**. Validation of selected SLC/drug associations by MCA. Results are shown by gene tested, pooling data of 1-5 independent experiments (biological replicates) each performed in technical triplicates. Ratios of GFP+/mCherry+ populations normalized to day0 ratios are shown for the indicated SLC/drug combinations at the given timepoints for the two sgRNAs tested, with different point shapes corresponding to separate biological replicates. Bars correspond to mean of all measurements shown. Statistical significance was calculated by ANOVA using biological replicates followed by Dunnett's test. Compounds tested: ART: Artesunate, DHA: Dihydroartemisinin, NIS: Nisoldipine, PEN: Pentamidine, MTX: Methotrexate, PDX: Pralatrexate, RTX: Raltitrexed, TOP: Topotecan, 5-AZA: 5-Azacytidine, DAC: Decitabine, ARA-C: Cytarabine, GEM: Gemcitabine, CDDP: Cisplatin. Controls: DMSO: Dimethyl sulfoxide, DMF: Dimethylformamide.

Europe PMC Funders Author Manuscripts

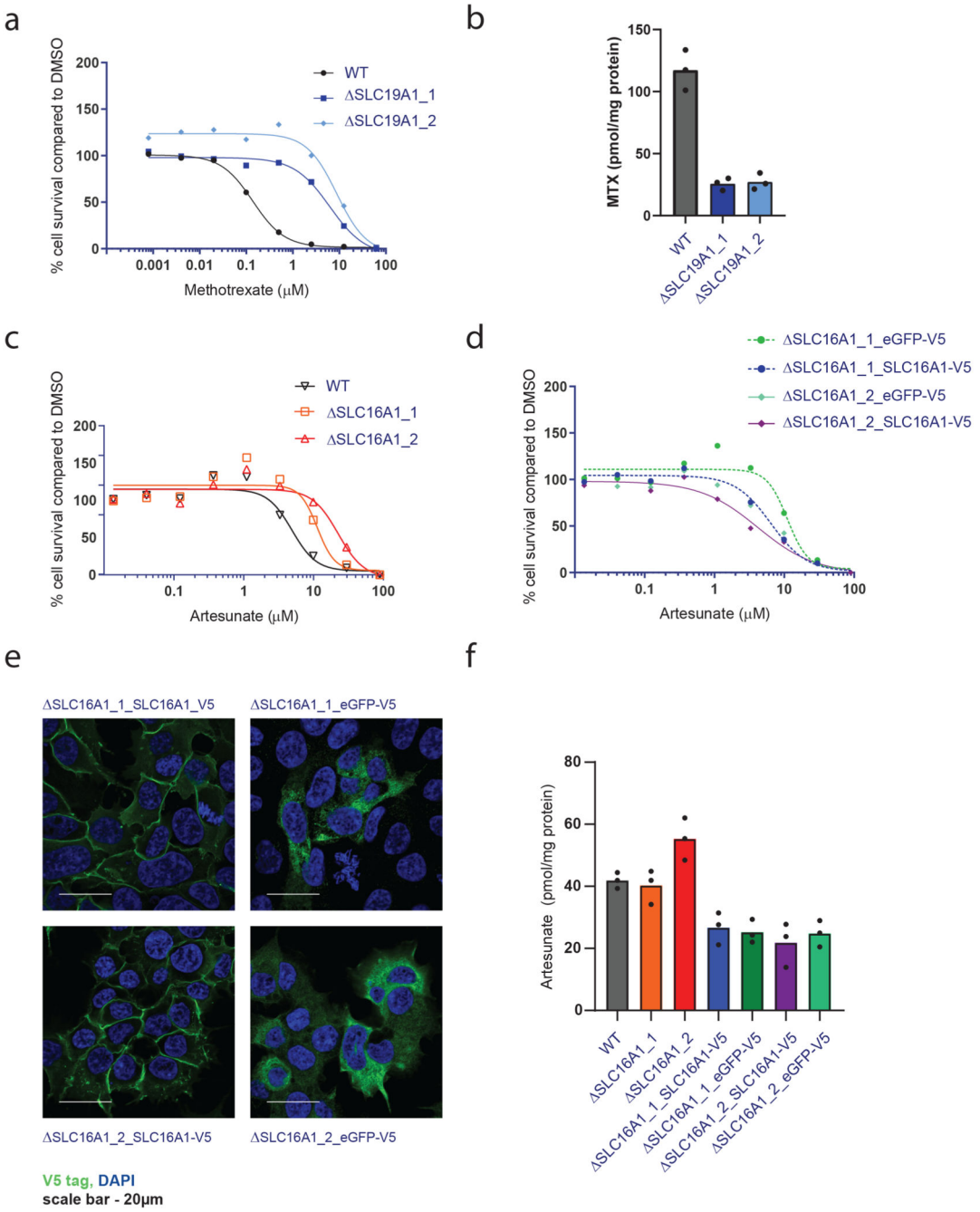

Figure 4.

a. Cell viability assay comparing sensitivity to methotrexate of WT HAP1 cells and cells carrying frameshift mutations in the SLC19A1 gene (ΔSLC19A1_1, ΔSLC19A1_2). Average values of three measurements are shown for a representative experiment (n=1). **b**. LC-MS/MS-based assay to measure intracellular concentrations of methotrexate in WT HAP1 cells and cells carrying frameshift mutations in the SLC19A1 gene (ΔSLC19A1_1, ΔSLC19A1_2). Bars show average of three measurements for a representative experiment (n=1). **c**. Cell viability assay comparing sensitivity to artesunate of WT HAP1 cells and cells

carrying frameshift mutations in the SLC16A1 gene (ΔSLC16A1_1, ΔSLC16A1_2). Average values of three measurements are shown for a representative experiment (n=1). **d**. Cell viability assay showing increased sensitivity of HAP1 SLC16A1 KO cells reconstituted with SLC16A1 cDNA compared to cells reconstituted with eGFP. Average values of three measurements are shown for a representative experiment (n=1). **e**. Confocal images of HAP1 cells lacking endogenous SLC16A1 and reconstituted with GFP or SLC16A1 cDNA. Green: eGFP or SLC16A1, Blue: DAPI. Scale bar: 20 μm. Representative images from one of two independent experiments performed. **f**. LC-MS/MS-based assay to measure intracellular concentrations of artesunate in WT HAP1 cells and cells with mutations in, or reconstituted with, the SLC16A1 cDNA. Bars show average of three measurements for a representative experiment (n=1). All experiments shown are representative of at least two independent measurements.

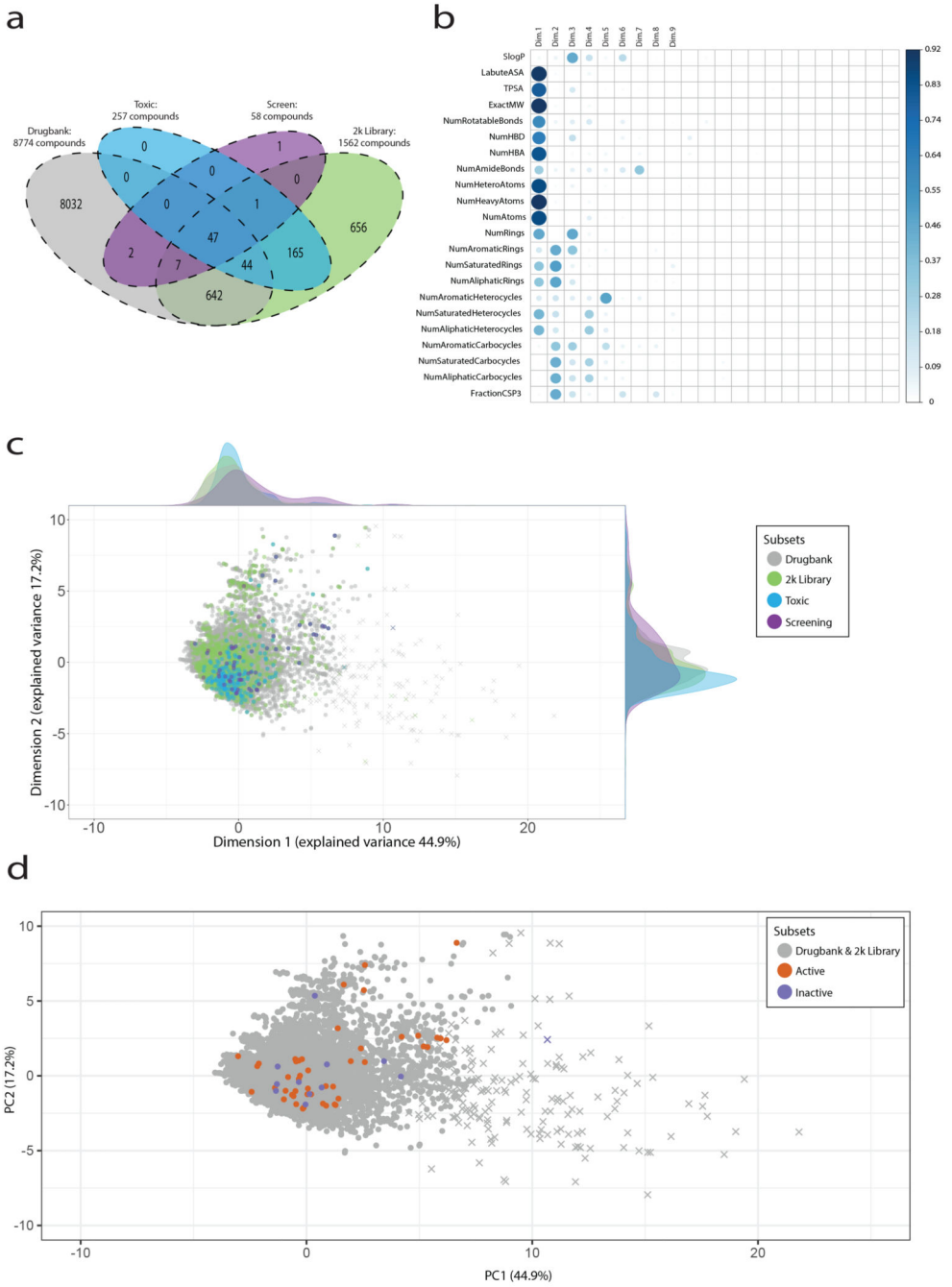

Figure 5.

a. Venn diagram showing the compound subsets used for the chemoinformatic analysis after stripping of stereochemistry and removal of anorganic and duplicated compounds. **b**. Correlogram plot showing the 2D descriptors contribution to the PCA analysis (n=9597). **c**. Principal components analysis of compounds in the DrugBank set of reference as well as in the sets tested in this study based on 22 annotated 2D chemical descriptors. The adjunct density plots show the distribution of compounds for Dimension 1 and Dimension 2. Compounds with a molecular weight below 900 Da (defined as “small molecule” by

Europe PMC Funders Author Manuscripts

DrugBank) are shown as circles, the remaining compounds as crosses. Sample size as in panel a. **d**. Principal components analysis of compounds in the DrugBank set of reference compared the SLC-associated (active, 47) and non-SLC-associated (inactive, 11) compounds based on 22 annotated 2D chemical descriptors. Zoomed-in version for clarity, the full plot is shown in Supplementary Fig. 5b.

Europe PMC Funders Author Manuscripts